Polarisation dynamics of a birefringent Fabry-Perot cavity

Aldo Ejlli[1]**, Federico Della Valle**[2,3]**, Guido Zavattini**[1]

[1] INFN, Sez. di Ferrara and Dip. di Fisica e Scienze della Terra, Università di Ferrara, via Saragat 1, Edificio C, I-44122 Ferrara, Italy

[2] INFN, Sez. di Trieste and Dip. di Fisica, Università di Trieste, via A. Valerio 2, I-34127 Trieste, Italy

[3] e-mail: federico.dellavalle@ts.infn.it

Abstract Optical Fabry-Perot cavities always show a non-degeneracy of two orthogonal polarisation states. This is due to the unavoidable birefringence of dielectric mirrors whose effects are extremely important in Fabry-Perot based high-accuracy polarimeters. We have developed and present here a theory of the polarisation state dynamics in a birefringent Fabry-Perot resonator, and we validate it through measurements performed with the polarimeter of the PVLAS experiment. The measurements are performed while a laser is frequency-locked to the cavity, and provide values for the finesse of the cavity and for the phase difference between the two orthogonal polarisation components introduced by the combination of the

two cavity mirrors (equivalent wave-plate). The theoretical formulas and the experimental data agree well showing that the consequences of the mirror birefringence must be taken into account in this and in any other similar experiment.

1 Introduction

Today high finesse Fabry-Perot (FP) cavities are often used to increase the effective optical path length of light within a given region. One such application is in very sensitive polarimetry [1,2,3,4]. Typically, to further increase the sensitivity of such an apparatus, the effect to be measured is modulated in time. Finesses have become so high that more and more often the modulated effect has frequency components close to or above the frequency cutoff of the cavity itself. For example, in ellipticity measurements, such Fabry-Perot cavities are treated as first order filters [5,6]. A complication exists when the mirrors of the Fabry-Perot cavity are birefringent, in that not only does the ellipticity generate a rotation [1,7] but the ellipticity and the rotation have different frequency responses, which depend on the cavity intrinsic birefringence.

In this paper we present an experimental method to make a complete characterisation of the polarisation dynamics of a Fabry-Perot cavity used for polarimetry. The study should be of interest for the wide community that employs Fabry-Perot cavities to pursue measurements of fundamental physics.

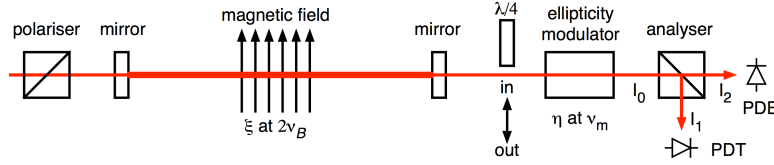## 2 Polarimetry with a birefringent cavity

2.1 General method

Fig. 1 Principle scheme for magneto-optical polarimetry with a Fabry-Perot cavity. PDT: transmission photodiode that collects the intensity I_1 of the electric field component with polarisation equal to that of the input light; PDE: extinguished beam photodiode that collects the intensity I_2 of the orthogonal component.

In previous papers $[1, 8, 9, 10, 11, 12, 13, 14]$, the method employed by the PVLAS experiment for ultra-high-sensitive magneto-optical polarimetry based on a Fabry-Perot (FP) cavity was presented. The instrument is a Malus interferometer [15], namely a Fabry-Perot cavity inserted between two crossed polarisers, with heterodyne detection [8]. The principle scheme is shown in Fig. 1. The instrument measures the ellipticity and the rotation acquired by linearly polarised light as a consequence of a magnetic anisotropy of the complex index of refraction $\tilde{n} = n + i\kappa$ of the medium between the mirrors. The ellipticity is the ratio of the minor to the major axis of the ellipse described by the electric field vector. With respect to the axes of the ellipse, there is a phase difference of $\pi/2$ between the two orthogonal components of the electric field: if the component of the electric field along the major

axis is real, the orthogonal component is a purely imaginary number. Differently, in rotations the two components remain in phase. We also remind the reader that, if all acquired ellipticities and rotations are small, then they add algebraically.

The most general element describing linear magnetic birefringence and dichroism can be expressed as a Jones matrix [16] as

$$\begin{pmatrix} e^{\xi/2} & 0 \\ 0 & e^{-\xi/2} \end{pmatrix},$$

where $\xi = i2\psi + 2\theta$; an overall attenuation factor has been neglected. The ellipticity ψ and the rotation θ acquired in a single passage through the magnetic region of length L are given by

$$\psi = \pi \frac{\Delta n L}{\lambda} \sin 2\phi \equiv \psi_0 \sin 2\phi \qquad \text{and} \qquad \theta = \pi \frac{\Delta \kappa L}{\lambda} \sin 2\phi \equiv \theta_0 \sin 2\phi,$$

where λ is the light wavelength, $\Delta n = n_{\parallel} - n_{\perp}$ is the magnetic birefringence, $\Delta \kappa = \kappa_{\parallel} - \kappa_{\perp}$ is the magnetic dichroism and ϕ is the angle between the input polarisation direction (electric field of the light beam) and the external magnetic field. The subscripts $\parallel$ and $\perp$ refer to the direction of the external magnetic field. In the PVLAS experiment, rotating the dipole permanent magnets that generate the magnetic field modulates the magneto-optical effects; an ellipticity modulator is used for heterodyne detection. If a quarter-wave plate is properly inserted between the output mirror and the modulator, so as to transform rotations into ellipticities, rotation measurements are obtained. If the $\lambda/4$ plate is not inserted, ellipticity is measured. Indeed, the ellipticity of the modulator will only beat with other ellipticities.

The Fabry-Perot lengthens the optical path within the interaction region thus amplifying both the ellipticity and the rotation by a factor $N = 2\mathcal{F}/\pi$, where $\mathcal{F}$ is the finesse of the cavity given by [17]

$$\mathcal{F} = \frac{\pi\sqrt{R}}{1-R}, \tag{1}$$

with R the reflectance of the cavity mirrors, assumed identical. Finesse values cas high as 7.7×10^5 can be obtained [18]. We denote with

$$\Psi = N\psi \equiv \Psi_0 \sin 2\phi \qquad \text{and} \qquad \Theta = N\theta \equiv \Theta_0 \sin 2\phi$$

the amplified values of the ellipticity and of the rotation. Let us indicate with $\eta(t) = \eta_0 \sin \omega_\mathrm{m} t$ with $\eta_0 \ll 1$ the ellipticity introduced by the ellipticity modulator and let us assume that $\eta_0 \gg \Psi_0, \Theta_0$. In the presence of both rotations and ellipticities, the extinguished intensity collected by the photodiode PDE in the ellipticity measurements and rotation measurements is given by

$$I_2^\mathrm{ell} = I_0 \left[\sigma^2 + |i\eta + i\Psi + \Theta|^2 \right]$$
$$I_2^\mathrm{rot} = I_0 \left[\sigma^2 + |i\eta + i\Theta + \Psi|^2 \right], \tag{2}$$

where σ^2 is the extinction coefficient of the crossed polarisers and I_0 is the intensity transmitted by the cavity, essentially equal to the intensity I_1 collected by photodiode PDT. The values of ellipticity or rotation are extracted from a Fourier transform of the extinguished intensity. Indicating with ν_B the rotation frequency of the magnets and with ν_m the modulation frequency of the ellipticity it can be seen, by inspection of Eqs. (2), that the

amplitude of the Fourier components at the frequencies $\nu_\mathrm{m} \pm 2\nu_B$ is linear in the ellipticity or in the rotation, Ψ_0 or Θ_0, respectively [8,11]:

$$I^\mathrm{ell}_{\nu_\mathrm{m} \pm 2\nu_B} = I_0\, 2\, \eta_0\, \Psi_0 \qquad \text{or} \qquad I^\mathrm{rot}_{\nu_\mathrm{m} \pm 2\nu_B} = I_0\, 2\, \eta_0\, \Theta_0.$$

By demodulating the extinguished intensity at the frequency ν_m, the ellipticity and rotation signals can be expressed in terms of the components of the Fourier transform of the demodulated signal as [1]

$$\Psi_0, \Theta_0 = \frac{I_{2\nu_B}}{2\sqrt{2\, I_0\, I_{2\nu_\mathrm{m}}}}. \tag{3}$$

2.2 Birefringent mirrors

In previous papers [1,7] it was shown that, as a consequence of the intrinsic birefringence of the cavity mirrors [19], a cross-talk between ellipticity and rotation arises. We are assuming that a laser is frequency-locked to a birefringent cavity and that the input polarisation is aligned with one of the axes of the equivalent wave-plate of the cavity. In the case in which only an ellipticity is generated (pure Cotton-Mouton – or Voigt – effect in gases [20]) the electric field component with orthogonal polarisation can be written as

$$E_{\mathrm{out},2}(\phi) = i\, \Psi_0\, k(\alpha) \left(\frac{E_0 T}{1 - R} \right) \left(1 - i\, \frac{N}{2}\, \sin\alpha \right) \sin 2\phi,$$

where T is the transmittance of the mirrors, α is the total phase difference (due to the two mirrors) acquired by the two orthogonal polarisation components in a cavity round trip, and

$$k(\alpha) = \frac{1}{1 + N^2 \sin^2(\alpha/2)}$$

is a factor taking into account the fact that, since the extinguished beam experiences a phase shift in the reflection on the mirrors, it cannot be on top of the cavity resonance curve. The electric field has an imaginary component describing the induced ellipticity but also a real component describing a rotation. More in general, in the presence of both an ellipticity $\Psi_0 = N\psi_0$ and a rotation $\Theta_0 = N\theta_0$ the measured values of Ψ and Θ are respectively

$$\Psi = k(\alpha) \left[\Psi_0 - \frac{N\alpha}{2}\Theta_0\right] \qquad \text{and} \qquad \Theta = k(\alpha) \left[\Theta_0 + \frac{N\alpha}{2}\Psi_0\right]. \quad (4)$$

This means that, if the cavity mirrors are birefringent (and they always are), no meaningful measurement of only ellipticity or rotation can be done. By measuring both, instead, the values of Ψ_0 and Θ_0 can in principle be disentangled by solving the two equations (4) above, provided that N and α are known. These two parameters completely characterise a Fabry-Perot cavity when used as a polarimetric device. In this paper we present a simple method to measure the two parameters.

A measurement of N is normally obtained by measuring the decay time τ_I of the intensity transmitted by the cavity, recorded by the photodiode PDT of Fig. 1:

$$\tau_I = \frac{Nd}{2c}, \quad (5)$$

where d is the distance between the cavity mirrors. This measurement usually implies unlocking the laser. In order to measure α, one has to resort to experimental configurations in which a birefringence and a dichroism are not simultaneously present. In these cases, in fact, only one of the two

quantities ψ_0 and θ_0 are different from zero. If for example $\theta_0 = 0$ (pure birefringence, as in gases) one has

$$\Psi_{\mathrm{b}} = k(\alpha)\, \Psi_0 \qquad \text{and} \qquad \Theta_{\mathrm{b}} = k(\alpha)\, \frac{N\alpha}{2}\, \Psi_0. \tag{6}$$

The ratio of the rotation Θ_b and of the ellipticity Ψ_b is then

$$R_0 = \frac{\Theta_b}{\Psi_b} = \frac{N\alpha}{2}, \tag{7}$$

giving the value of α. The same mathematics applies to the complementary case in which only $\theta_0 \neq 0$ (a pure dichroism – or, more generally, a rotation):

$$\Theta_{\mathrm{d}} = k(\alpha)\, \Theta_0 \qquad \text{and} \qquad \Psi_{\mathrm{d}} = k(\alpha)\, \frac{N\alpha}{2}\, \Theta_0. \tag{8}$$

The ratio Ψ_d/Θ_d gives the same value of R_0.

2.3 Frequency dependence

When doing polarimetry with a Fabry-Perot cavity, since the mirrors in practice always feature some birefringence, one has to pay attention to the different frequency dependences of the two terms appearing in each of the two equations (4). As the effects are modulated by the rotation of the magnetic field, these equations concern the amplitude of Fourier components of the extinguished intensity, and not dc quantities: the equations (4) strictly hold only in the limit of zero frequency. The first term in each of the two equations (4) has the same frequency dependence as the electric field transmitted by the cavity, namely that of a first order filter [5]. The second terms in the two equations, instead, are generated by a second order process. In

fact, in order for them to show up, the polarisation component orthogonal to the input polarisation must first be created and only then the effect of the intrinsic birefringence of the mirrors can transform the ellipticity into a rotation and *vice versa*.
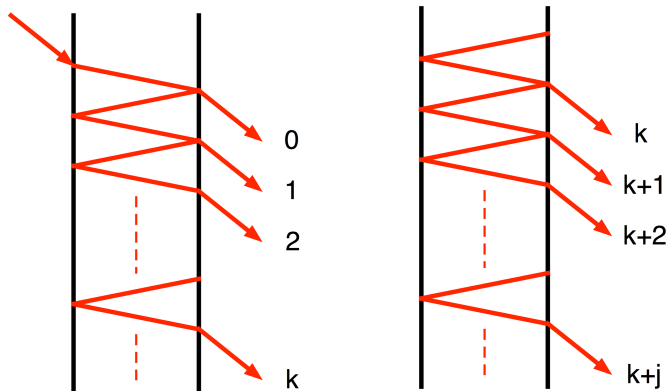

Fig. 2 Fabry-Perot cavity used for magnetic polarimetry, schematised as a multiple interference phenomenon. The incidence angle is shown as non-zero only for the sake of the argument; it is brought to zero at the end of the calculation. Left: transmitted beam; Right: extinguished beam.

A more detailed analysis of the phenomenon shows that the non-zero value of α modifies the frequency response of the two signals with respect to the simple first and second order filters. The calculation is performed referring to the usual scheme of multiple interference depicted in Fig. 2, applied to the two cavities, one travelled by light having polarisation equal to the input one, and the other with orthogonal polarisation. The two cavities coincide spatially, but do not interfere. The second cavity has no input

beam, and is pumped by the magnetic anisotropy. We analyse the case of
the magnetic birefringence that is generated by the rotating magnetic field
in gas; the specular case of the dichroism can be treated exactly with the
same mathematics. The magnetic birefringence due to the rotating magnets
can be schematised as a rotating birefringent wave-plate with a small phase
difference $2\psi_0 \ll 1$ (as we will see, one must have $N\psi_0 \ll 1$). This corre-
sponds to a maximum ellipticity per passage equal to ψ_0. As said above,
light in the first cavity is kept on top of the resonance curve by means of a
feedback system that locks the laser frequency to the resonance frequency
of this cavity. This amounts to say that the multiple beam pattern on the
left of Fig. 2 is stationary, and not time dependent. In this condition, the
electric field at the exit of this cavity is easily calculated as

$$E_{\text{out},1} = E_0 T \left(1 + R + R^2 + ... + R^k + ... \right) = \frac{E_0 T}{1 - R} = E_0 T \, \frac{N}{2},$$

where R is the reflectance of the mirrors. To calculate the behaviour of
the second cavity with orthogonal polarisation, we focus on the k-th pair
of passages inside the first cavity, with an electric field $\approx E_0 \sqrt{T} R^k$. The
beam traverses two times the birefringent region, giving a contribution to
the electric field inside the second cavity equal, to first order in ψ_0, to
$2i\psi_0 \sin 2\phi \, E_0 \sqrt{T} R^k$, where $\phi = \omega_B t + \phi_0$ is the time dependent angle be-
tween the input polarisation direction and the instantaneous direction of
the magnetic field. This contribution exits the second cavity by undergoing
multiple reflections, during which a negligible ellipticity is generated back
in the first cavity. To synchronise all the partial beams in the output electric

field, however, one has to consider contributions that have been generated at previous times separated by the time interval $\tau = 2d/c$. The electric field at the exit of the second cavity is then given by

$$
E_{\text{out},2}(\phi) \approx 2i\psi_0 E_0 T \sum_k R^k \sum_j R^j e^{-ji\alpha} \sin 2\phi_j =
$$

$$
= E_0 \frac{T\psi_0}{1-R} \left[\frac{e^{2i\phi}}{1 - Re^{-i\alpha}e^{2i\omega_B\tau}} - \frac{e^{-2i\phi}}{1 - Re^{-i\alpha}e^{-2i\omega_B\tau}} \right],
$$

where $\phi_j = \phi - j\omega_B\tau$. In this second cavity, the phase factor $e^{-i\alpha}$ is introduced at each round trip to take into account the birefringence of the cavity mirrors: remember that the polarisation is aligned to one of the cavity axes.

Using the Jones matrices, the electric field at the photodiode PDE is obtained as

$$
\mathbf{E}(\phi) = \begin{pmatrix} 0 & 0 \\ 0 & 1 \end{pmatrix} \cdot \begin{pmatrix} 1 & i\eta \\ i\eta & 1 \end{pmatrix} \cdot \begin{pmatrix} q & 0 \\ 0 & q^* \end{pmatrix} \cdot \begin{pmatrix} E_{\text{out},1} \\ E_{\text{out},2} \end{pmatrix}.
$$

In this formula, from left to right, one finds the matrices of the analyser, of the ellipticity modulator, and of the quarter-wave-plate. In this last matrix, $q = 1$ for ellipticity measurements, when the wave-plate is out of the optical path and the matrix therefore coincides with the identity matrix, whereas $q = (1+i)/\sqrt{2}$ for rotation measurements when the quarter wave-plate is inserted. The extinguished electric field is then

$$
E_2(\phi) = \frac{E_0 T}{1-R} \left[iq\eta + q^* \psi_0 \left(\frac{e^{2i\phi}}{1 - Re^{-i\alpha}e^{2i\omega_B\tau}} - \frac{e^{-2i\phi}}{1 - Re^{-i\alpha}e^{-2i\omega_B\tau}} \right) \right].
$$

By Fourier transforming the intensity recorded by the photodiode PDE demodulated at the frequency ν_{m} of the ellipticity modulator, and by substituting $2\omega_B$ with a generic signal angular frequency $2\pi\nu$, one is able to

obtain the values of the ellipticity Ψ_b and of the rotation Θ_b by making reference to Eq. (3). The results of the calculation are expressed as amplitude and phase:

$$|\Psi_b| = \frac{T^2}{(1-R)^2} \sqrt{\frac{16\,\psi_0^2\,[1 - R\cos\alpha(2\cos\delta - R\cos\alpha)]}{[1 + R^2 - 2R\cos(\alpha - \delta)]\,[1 + R^2 - 2R\cos(\alpha + \delta)]}}$$

$$\arg(\Psi_b) = \arctan\left[\frac{-R\left[(1 + R^2)\cos\alpha - 2R\cos\delta\right]\sin\delta}{1 + R^2 + R\left[R\cos 2\alpha - (3 + R^2)\cos\alpha\cos\delta + R\cos 2\delta\right]}\right]$$

$$|\Theta_b| = \frac{T^2}{(1-R)^2} \sqrt{\frac{16\,\psi_0^2\,R^2\sin^2\alpha}{[1 + R^2 - 2R\cos(\alpha - \delta)]\,[1 + R^2 - 2R\cos(\alpha + \delta)]}}$$

$$\arg(\Theta_b) = \arctan\left[\frac{-2R\cos\alpha + (1 + R^2)\cos\delta}{(1 - R^2)\sin\delta}\right], \tag{9}$$

where $\delta = 2\pi\nu\tau$. The formulas for the case of the dichroism are obtained from the ones above substituting Ψ_b with Θ_d, Θ_b with Ψ_d and ψ_0 with θ_0:

$$|\Theta_d| = \frac{T^2}{(1-R)^2} \sqrt{\frac{16\,\theta_0^2\,[1 - R\cos\alpha(2\cos\delta - R\cos\alpha)]}{[1 + R^2 - 2R\cos(\alpha - \delta)]\,[1 + R^2 - 2R\cos(\alpha + \delta)]}}$$

$$\arg(\Theta_d) = \arctan\left[\frac{-R\left[(1 + R^2)\cos\alpha - 2R\cos\delta\right]\sin\delta}{1 + R^2 + R\left[R\cos 2\alpha - (3 + R^2)\cos\alpha\cos\delta + R\cos 2\delta\right]}\right]$$

$$|\Psi_d| = \frac{T^2}{(1-R)^2} \sqrt{\frac{16\,\theta_0^2\,R^2\sin^2\alpha}{[1 + R^2 - 2R\cos(\alpha - \delta)]\,[1 + R^2 - 2R\cos(\alpha + \delta)]}}$$

$$\arg(\Psi_d) = \arctan\left[\frac{-2R\cos\alpha + (1 + R^2)\cos\delta}{(1 - R^2)\sin\delta}\right]. \tag{10}$$

It is easy to verify that the formulas (6) and (8) are obtained from the amplitudes in the limit $\delta \to 0$.

In Fig. 3, the four equations (9) above are plotted as functions of the frequency for various values of $R_0 = N\alpha/2$. In the limit $R_0 \to 0$, the transfer function of the ellipticity reduces to that of a first order filter [5]:

$$\lim_{R_0 \to 0} |\Psi_d| \propto \frac{T}{\sqrt{1 + R^2 - 2R\cos\delta}} = h_{\mathrm{T}}(\nu)$$

$$\lim_{R_0 \to 0} \arg(\Psi_d) = \arctan\left[\frac{R\sin\delta}{1 - R\cos\delta}\right] = \phi_{\mathrm{T}}(\nu). \tag{11}$$
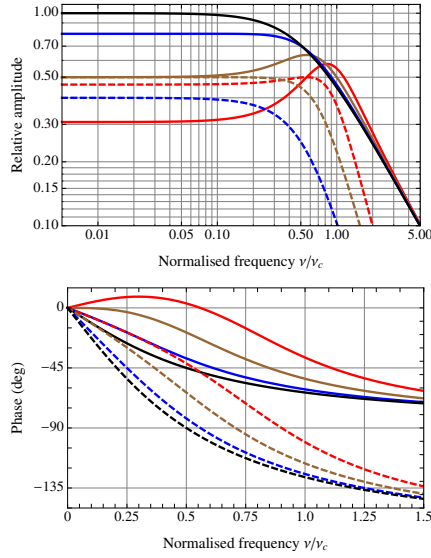
Fig. 3 Top panel: Calculated frequency response of the amplitude of the ellipticity (continuous curves) and of the rotation (dashed curves) generated by magnetic birefringence in gas in the PVLAS polarimeter, employing a high-finesse Fabry-Perot cavity with birefringent mirrors. The frequency scale is expressed in units of the cavity line-width ν_c; the vertical scale is normalised to the low-frequency amplitude of the $R_0 = 0$ filter [Eq. (11)]. The ellipticity curves are drawn for the values of the low-frequency ratio of rotation to ellipticity [Eq. (7)] $R_0 = 0$, 0.5, 1.0 and 1.5; the rotation curves have $R_0 = 0.5$, 1.0 and 1.5. Bottom panel: Calculated frequency response of the phase of the ellipticity (continuous curves) and of the rotation (dashed curves), drawn for the values of $R_0 = 0$, 0.5, 1.0 and 1.5. The curves have been arbitrarily chosen to start at zero phase and have negative slope.

In the same limit, the rotation amplitude vanishes; nevertheless, for small R_0, the shape of the rotation curve and its phase converge to those of a

second order filter:

$$H_{\text{T}}(\nu) = h_{\text{T}}^2(\nu) \qquad \text{and} \qquad \Phi_{\text{T}}(\nu) = 2\phi_{\text{T}}(\nu). \qquad (12)$$

In this article we present an experimental study of the Fabry-Perot cavity of the PVLAS polarimeter, obtained through the measurements of two magneto-optical effects as a function of frequency. One is the magnetic birefringence in gas. The second is the rotation generated by a Faraday effect in the reflecting layers of the dielectric mirrors of the cavity [21]; for this second measurement, a solenoid coil has been added to the PVLAS apparatus. The choice of the Faraday effect is motivated by the absence of a usable low-energy magnetic dichroism effect in gases. Each of the two sets of data is a complete characterisation of the FP cavity. Both confirm the frequency dependences quoted above.

3 Experimental set-up and method

3.1 The PVLAS polarimeter

The set-up of the PVLAS has been presented elsewhere [1], hence only a brief summary will be given here. A scheme and a picture of the apparatus are shown in Fig. 4. The polarimeter consists of a 3.3 m long Fabry-Perot cavity inserted between two crossed polarisers. The finesse of the cavity has been measured recording the decay of the intensity I_1. The results are reported in Fig. 5. The best fit gives $\tau_I = 2.32 \pm 0.02$ ms, corresponding to a finesse $\mathcal{F} = (662 \pm 6) \times 10^3$, $N = (421 \pm 4) \times 10^3$ and a line-width
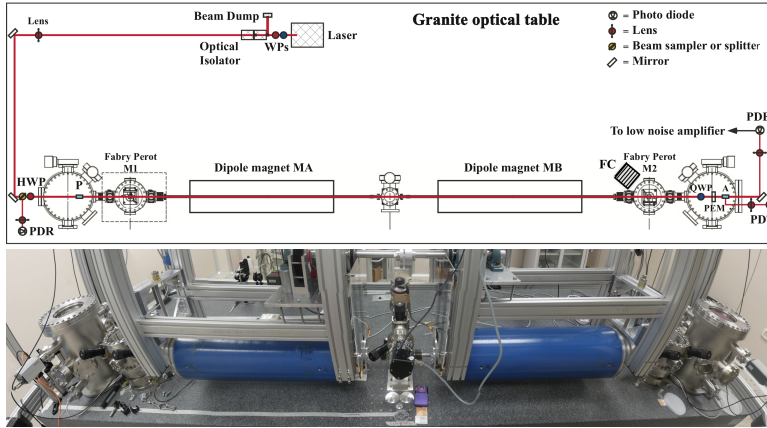
Fig. 4 Top: optical scheme of the apparatus. WPs = Wave-plates; HWP = Half-wave-plate; PDR = Reflection photodiode; P = Polariser; Ms = Mirrors; QWP = Quarter-wave-plate; PEM = Photoelastic modulator; A = Analyser; PDT = Transmission photodiode; PDE = Extinction photodiode; FC = Faraday coil. Bottom: a picture of the experiment. The two blue cylinders are the dipole magnets.

$\nu_c = 68.0\pm0.6$ Hz. The whole polarimeter, from the polariser to the analyser is kept in high vacuum (pressure better than 10^{-7} mbar) or in a pure gas at low pressure. We have verified that the value of the finesse does not change due to the presence of the gas. The light source is a 2 W tuneable laser, frequency-locked to the cavity using the Pound-Drever-Hall method [22]. In the cavity, the beam travels inside glass tubes traversing the bores of two identical dipole permanent magnets (magnetic field lines orthogonal to the light path). The magnetic field inside each 20 mm diameter bore is 2.5 T, each magnetic region having an effective length $L = 0.82$ cm long [1]. The magnets rotate around their axes; this modulates both the magnetic
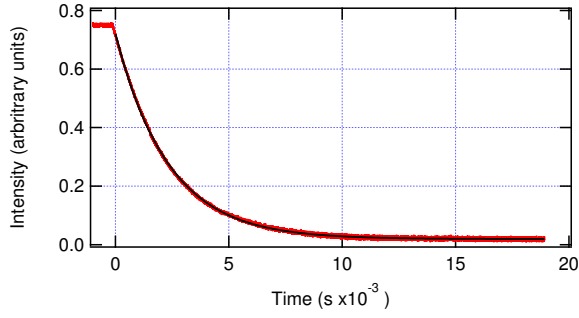
Fig. 5 Decay of the intensity I_1 transmitted by the Fabry-Perot cavity following switching off of the system that locks the frequencies of the laser and the cavity. The experimental curve is fitted with an exponential function $Ae^{-t/\tau_I} + C$ with $\tau_I = 2.32$ ms, corresponding to a finesse $\mathcal{F} = 662 \times 10^3$.

birefringence and the dichroism at twice the rotation frequency. Before the analyser, a small ellipticity, modulated at $\nu_{\mathrm{m}} = 50$ kHz, is added to the beam polarisation by means of a Photo-Elastic Modulator (PEM). A retractable quarter-wave plate is inserted between the FP and the PEM during the rotation measurements. After the analyser, the extraordinary beam and the extinguished one are collected on two photodiodes. The extinguished intensity is demodulated at the frequency of modulation ν_{m}. The signal is then filtered, digitised and Fourier transformed.

3.2 The measurement method

In the work presented in this paper, two different measurement configurations have been used. In both configurations, the ellipticity signal Ψ and the rotation signal Θ have been measured, both in amplitude and phase, as

a function of the frequency. In the first configuration, one of the two rotating PVLAS magnets is used to induce a magnetic birefringence in Ar gas at 880 μbar (Cotton-Mouton effect [20]) at frequencies ranging from 1 to 46 Hz (magnet rotation frequencies from 0.5 to 23 Hz). The ellipticity and rotation signals are in this case described by Eqs. (9). In the second configuration, a solenoid coil, positioned outside the vacuum chamber hosting one of the cavity mirrors and roughly aiming at the mirror centre, is used to generate an alternating magnetic field with a significant component orthogonal to the reflecting surface of the mirror, thus generating a Faraday effect [21]. We analyse the data in the same frequency range as above. With a 1 A current, the coil produces a magnetic field ≈ 1 G at a distance of 15 cm from the mouth of the coil (distance to the mirror). Precise values of the magnitude and of the orientation of the magnetic field at the position where the light beam impinges on the mirror are unknown, but on the other hand unnecessary. Since in this second experiment the vacuum vessel is kept in vacuum, no gas birefringence is generated, and the measured rotation and ellipticity signals are given by Eqs. (10). In the case of the Cotton-Mouton effect, rotating the magnet at a frequency ν_B generates signals at frequency $2\nu_B$. In the case of the Faraday effect, a magnetic field oscillating at a frequency ν_F generates signals at the same frequency. In this case, the Frequency Response function of an Agilent 35670A Dynamic Signal Analyzer has been employed. The frequency response is obtained as the coherent average of fast 0.16 s/Hz sweeps over 400 points and 50 Hz frequency range. In the

case of the Cotton-Mouton effect, the phases of the signals are measured with respect to a trigger signal generated by a contrast sensitive diode in correspondence of the passage of a mark drawn on the external surface of the rotating magnet. The diode has a response time $< 50~\mu$s, corresponding to a maximum phase uncertainty $< 0.8°$ at 46 Hz. Note that the resulting phases depend on the angle between the polarisation direction and the diode position. In the case of the Faraday effect, the phases are measured with respect to the current flowing through the coil. In both cases, a small correction has been subtracted from the measured phase, due to the frequency response of the lock-in amplifier used to demodulate the signal from the diode PDE collecting the extinguished intensity. The amplitude of the signals measured in the Faraday effect has been normalised to the intensity of the current in the coil.

4 Results and discussion

4.1 Magnetic birefringence in gas

In Fig. 6, the relative amplitude and phase of the ellipticity and rotation signals measured as a function of the frequency in the Cotton-Mouton effect of 880 μbar of Ar gas are shown. Integration time was 256 s/point for both ellipticity and rotation measurements. A constant phase, measuring the zero-frequency relative position of the signals and the trigger, has been subtracted from the phase data, so as to have both curves starting at zero phase. The experimental points are fitted simultaneously with the four func-
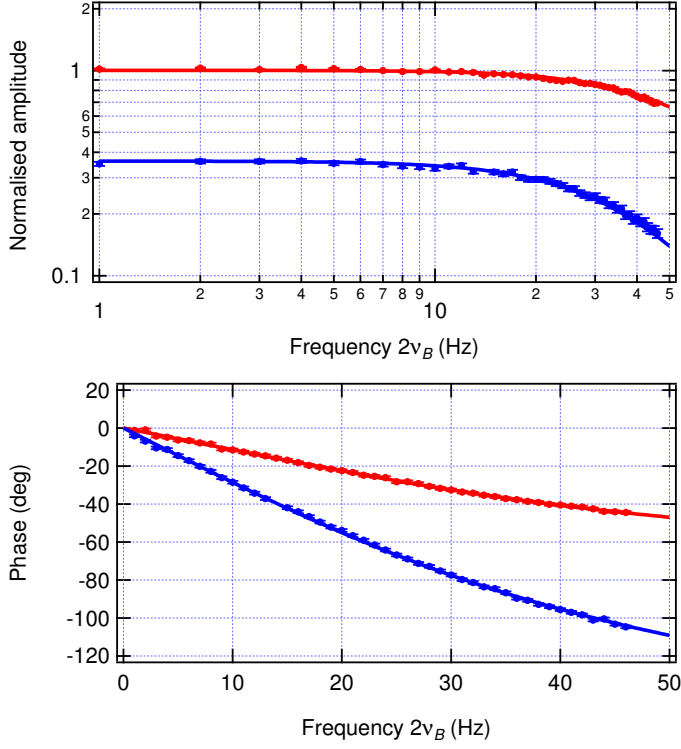
Fig. 6 Top panel: relative amplitude of the ellipticity signal Ψ_b (upper curve) and of the rotation signal Θ_b (lower curve) measured as a function of frequency for the Cotton-Mouton effect of 880 μbar of Ar gas. Bottom panel: phases of the ellipticity signal Ψ_b (upper curve) and of the rotation signal Θ_b (lower curve). The continuous lines are the global fit obtained with Eqs. (9). The values of the finesse $\mathcal{F}$ and of the phase difference α are obtained as $\mathcal{F} = 640 \times 10^3$ and $\alpha = 1.78$ μrad.

tions of Eqs. (9). The fit provides a unique value for the reflectance R and hence for the finesse $\mathcal{F}$ [see Eq. (1)], and for the phase difference α appearing in the expressions of the four curves. The values found are $\mathcal{F} = (640 \pm 4) \times 10^3$ and $\alpha = (1.78 \pm 0.02)$ μrad, with a normalised $\chi^2_{\text{o.d.f.}} = 181/174$. The value

obtained for the finesse is about 4% smaller than the value obtained from the analysis of the decay of the intensity transmitted by the FP cavity (see Fig. 5), and is compatible with that within three standard deviations. The uncertainties used in the fit are the piecewise standard deviations of the residuals obtained by fitting the four curves separately. In a first tentative of a global fit, the residuals of the phase data exhibited a marked linear behaviour of a few degrees over the whole frequency interval. This behaviour can be attributed to the fact that, during the measurements, the polarisation direction of the light entering the Fabry-Perot cavity is varied by small quantities to compensate for the slow drift of the static birefringence of the cavity. We have then added two linear functions to the two phase fit functions. The values of the slopes obtained through the fit are $(0.1° \pm 0.01°) \ \mathrm{Hz}^{-1}$ for the phase of the ellipticity, and $(0.05° \pm 0.01°) \ \mathrm{Hz}^{-1}$ for the phase of the rotation. Note that the duration of the ellipticity and rotation measurements were, respectively, eight hours and four hours, leading to an identical drift of 160 μdeg/s in the two measurements. This strongly supports the suggested interpretation. It is worth noting that the value of α is small enough that fitting simultaneously the four data sets with the expressions of the first and second order filters (11) and (12) still produces a reasonable fit, with a similar χ^2 probability, but at the expenses of an unreasonable 20% reduction of the value of $\mathcal{F}$ and of completely incompatible drifts of the ellipticity and rotation phases. In this case, α can be extracted

from the low frequency ratio R_0 of the amplitudes of rotation and ellipticity

[see Eq. (7)].

4.2 Magnetic rotation

In Fig. 7, the relative amplitude and phase of the rotation and ellipticity

signals measured as a function of the frequency ν_F of the current in the

Faraday coil are shown. Integration time was 18 s/point for the rotations

measurement, and 50 s/point for the ellipticity measurement. In this second

experiment, an alternating current with amplitude ≈ 1 A and frequency ν_F

sweeping between 0 and 50 Hz is fed to the coil FC of Fig. 4. The amplitude

data have been normalised to the current through the coil. A constant phase,

measuring the zero-frequency relative position of the signals and the trigger,

has been subtracted from the phase data, so as to have both curves starting

at zero phase. The experimental points are fitted with the four functions

of Eqs. (10). The fit provides a unique value for the finesse $\mathcal{F}$ and the

phase difference α appearing in the expressions of the four curves. The

values found are $\mathcal{F} = (691 \pm 8) \times 10^3$ and $\alpha = (1.87 \pm 0.02)$ μrad with a

normalised $\chi^2_{\text{o.d.f.}} = 1472/1434$. The value obtained for the finesse is about

4% larger than the value obtained from the analysis of the decay of the

intensity transmitted by the FP cavity (see Fig. 5), and is compatible with

that within three standard deviations. The value of α is 5% larger than the

one found in the Cotton-Mouton experiment described above; the two values

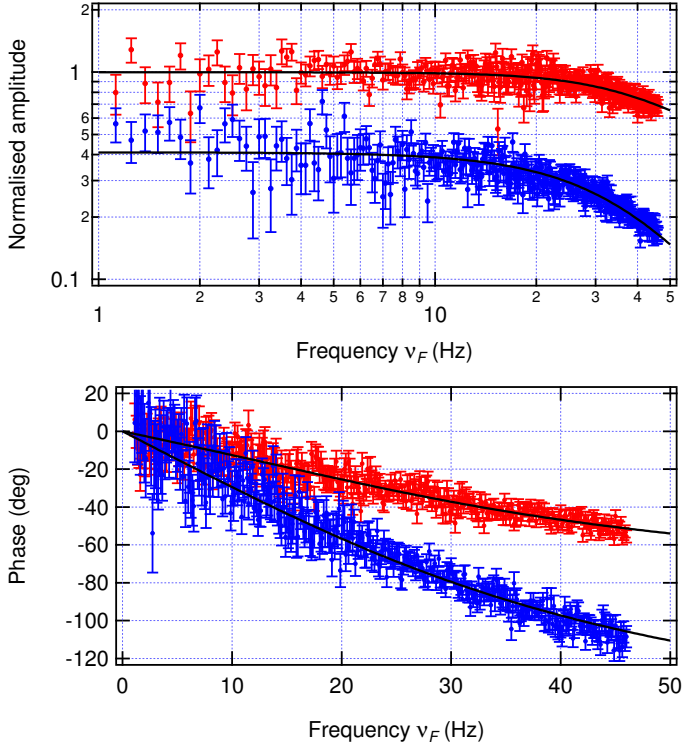are compatible within three standard deviations. This small difference could

Fig. 7 Top panel: relative amplitude of the rotation signal Θ_d (upper curve) and of the ellipticity signal Ψ_d (lower curve) measured as a function of frequency for the Faraday effect on the reflecting surface of a mirror of the FP cavity. Bottom panel: phases of the rotation signal Θ_d (upper curve) and of the ellipticity signal Ψ_d (lower curve). The continuous lines are the global fit obtained with Eqs. (10). The values of the finesse $\mathcal{F}$ and of the phase difference α are obtained as $\mathcal{F} = 691 \times 10^3$ and $\alpha = 1.87$ μrad.

be accounted for by the fact that the two datasets were taken in different days and that we know that α is subject to small drifts. As in the case of the Cotton-Mouton measurement, the uncertainties used in the fit are the piecewise standard deviations of the residuals obtained by fitting the

four curves separately. Differently from the Cotton-Mouton case, no linear addition to the phase fit function was necessary. This is consistent with the interpretation of the feature observed in the Cotton-Mouton effect: in fact, in the case of the Faraday measurements, the phase is electronically defined. By fitting the four curves with the expressions of the first and second order filters (11) and (12) we obtained $\mathcal{F} = 594 \times 10^3$, with a χ^2 probability of 5×10^{-3}, justifying the necessity of introducing the parameter α.

5 Conclusions

In this paper we have presented two experimental characterisations of an optical Fabry-Perot cavity used for polarimetry. The studies provide values for the finesse of the cavity and for the phase difference acquired by light upon reflection on the dielectric mirrors of the cavity. The measurements are performed while the laser is frequency-locked to the cavity. The data are analysed in terms of the frequency response of the ellipticity and rotation signals, whose theory is developed and presented. The theoretical frequency responses show a marked deformation from the expressions of the first and second order filters, reducing to these last expressions for $R_0 = \frac{N\alpha}{2} \ll 1$.

It should be noted that the Cotton-Mouton characterisation of the cavity requires introducing a gas in the Fabry-Perot enclosure whereas the Faraday characterisation is less intrusive as it requires no interventions on the Fabry-Perot. The Faraday effect on the mirrors can therefore be used to monitor R_0 during polarimetric measurements.

6 Acknowledgments

References

1. F. Della Valle *et al.* (PVLAS collaboration), Eur. Phys. J. C **76**, (2016) 24.

2. 2. S.-J. Chen, H.-H. Mei and W.-T. Ni (Q&A collaboration), Mod. Phys. Lett. A **22**, (2007) 2815.

3. A. Cadène, *et al.* (BMV collaboration), Eur. Phys. J. D **68**, (2014) 16.

4. X. Fan *et al.* (OVAL collaboration), arXiv:1705.00495v1.

5. N. Uehara and K. Ueda, Appl. Phys. B **61**, (1995) 9.

6. R. Berceau *et al.*, Appl. Phys. B **100**, (2010) 803.

7. G. Zavattini *et al.*, Appl. Phys. B **83**, (2006) 571.

8. E. Iacopini and E. Zavattini, Phys. Lett. **85B**, (1979) 151.

9. E. Iacopini *et al.*, Nuovo Cimento **61 B**, (1981) 21.

10. R. Cameron *et al.* (BFRT collaboration), Phys. Rev. D **47**, (1993) 3707.

11. D. Bakalov *et al.* (PVLAS collaboration), Quantum Semiclass. Opt. **10**, (1998) 239.

12. M. Bregant *et al.* (PVLAS collaboration), Phys. Rev. D **78**, (2008) 032006.

13. F. Della Valle *et al.* (PVLAS collaboration), New J. Phys. **15**, (2013) 053026.

14. F. Della Valle *et al.* (PVLAS collaboration), Phys. Rev. D **90**, (2014) 092003.

15. For a review of the Malus interferometer see M. Vallet *et al.*, Opt. Commun. **168**, (1999) 423.

16. R.C. Jones, J. Opt. Soc. Am. **38**, (1948) 671, and references therein.

17. M. Born and E. Wolf, *Principles of Optics* 6th ed. (Pergamon Press, Oxford 1989).

18. F. Della Valle *et al.*, Opt. Express **22**, (2014) 11570.

19. F. Brandi *et al.*, Appl. Phys. B **65**, (1997) 351.

20. For a review, see C. Rizzo, A. Rizzo and D.M. Bishop, Int. Rev. Phys. Chem. **16**, (1997) 81.

21. E. Iacopini, G. Stefanini and E. Zavattini, Appl. Phys. A **32**, (1983) 63.

22. G. Cantatore *et al.*, Rev. Sci. Instr. **66**, (1995) 2785, and references therein.